CHAPTER 4

THE PROPOSED PLL ASSISTED ADJUSTABLE SPEED CONTROL STRATEGY

4.1 Introduction

As discussed previously, the present issue of the PMBLDC motor drive mainly lies in the reduction of both manufacturing cost and the resulting electromagnetic torque ripples. In chapter 3, a solution toward cost reduction has been proposed and the resulting current-loop control is also able to reduce the commutation torque ripples greatly. In this chapter, further improvement in the speed control loop will be explored. Although, the PI speed controller has been popularly used in industry, however, due to the limited speed control accuracy, the resulting torque ripple can hardly be improved further for some high performance applications. On the other hand, instead of processing the speed error directly as the PI controller, a PLL control is able to provide much higher speed control accuracy by controlling the motor phase directly. In fact, the dual-mode PLL scheme [15] is based on the philosophy of combining both PI control and PLL control. Nevertheless, for variable speed control, due to the high inertia of the motor drive, it is rather difficult to maintain the locked condition under transient conditions. In view of these drawbacks, a novel PI type PLL speed control structure is proposed in section two which can obviate the controller structure change of the dual-mode PLL control as well as avoid the stability problem under transient conditions. Furthermore, to simplify the controller design, closed form expressions of the k_P and k_I parameters of the proposed PI controller are also derived based on the internal reference model control in section three. Finally, in the section 4.4, stability analysis of the closed loop system is also made and a stability criterion is also

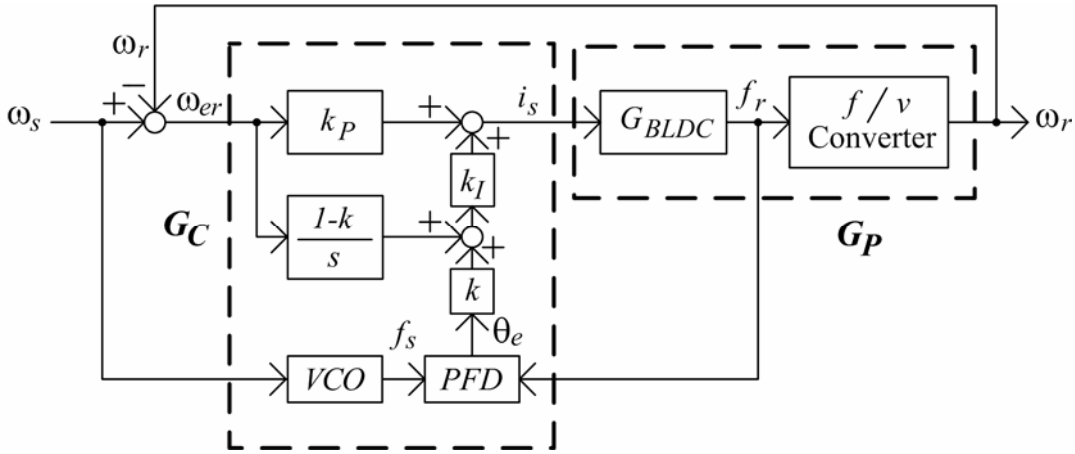

Fig. 4.1 The proposed PLL assisted speed controller of the PMBLDC drive.

proposed.

4.2 The Proposed PLL Assisted Speed Control Strategy

Although the proposed integrated current controller proposed in the previous chapter can greatly reduce the resulting torque ripples by simply controlling the equivalent armature current (i_{eq}), however, the corresponding current command (i_s) as shown in Fig. 3.8 is actually obtained from the speed controller. Thus, in order to achieve both fast transient response and high speed control accuracy, a PLL control is augmented with the conventional PI control. In addition, with a view to tracking stably the variable speed of the adjustable speed drive, proper coordination between the PI control and the added PLL control should be made. In view of the above objectives as well as the low cost consideration, the proposed PLL assisted speed controller is given in Fig. 4.1. From Fig. 4.1 one can see that the proposed control strategy possesses a very simple structure. Excluding the feedback of the analogue speed signal ω_r to generate the speed error ω_{er}, basically there are only two blocks, namely G_P and G_C blocks. In G_P block, the

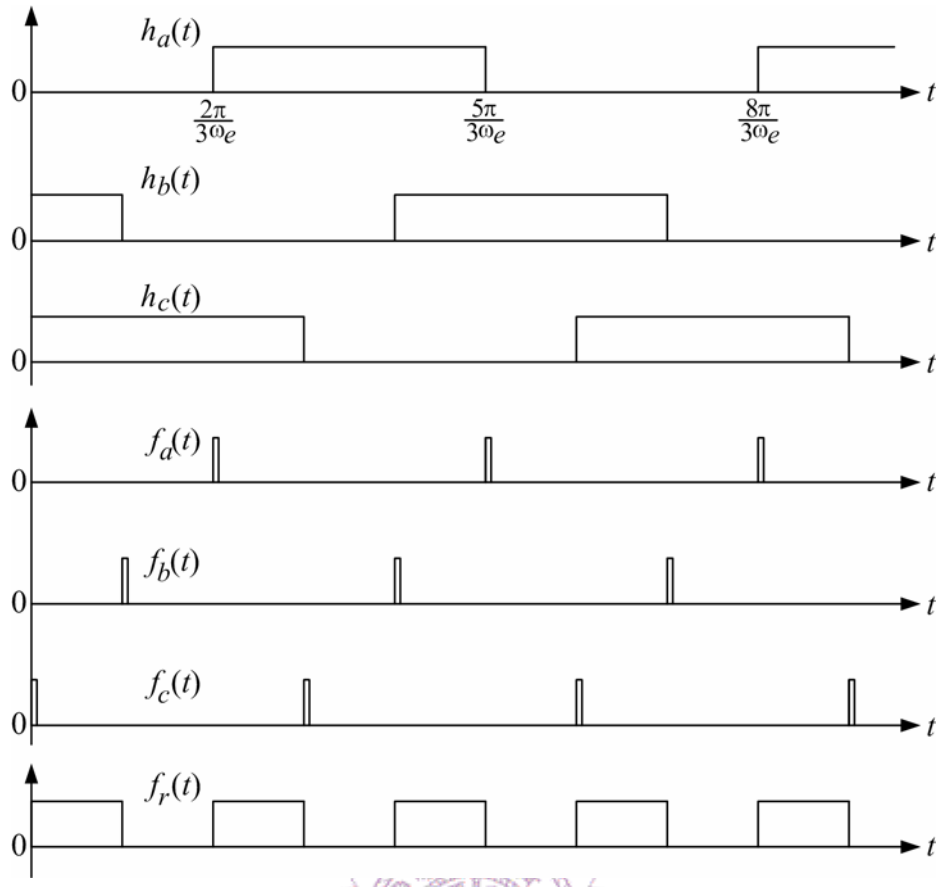

Fig. 4.2 The relationship between the Hall-sensor signals, h_a, h_b, h_c, the pulse signals, f_a, f_b, f_c and the motor speed pulse train signal f_r.

corresponding input i_s to output ω_r transfer function, namely $G_P(s)$, of the PMBLDC motor is given in (2.23). For convenient explanation, G_P is decomposed into parts, namely G_{BLDC} and the frequency to voltage converter (*f/v*). In G_P block, f_r is a pulse train signal representing the PMBLDC motor sped and is synthesized from the three Hall-sensor signals as shown in Fig. 4.2. From Fig. 4.2 one can see that all three Hall-sensor signals are first used to generate the f_a, f_b and f_c signals by detecting the rising and falling edges of three Hall-sensor signals. The f_r signal can then be synthesized from those signals as can be seen in Fig. 4.2. Application of all three Hall-sensor signals ill result in better speed response when motor speed is lower. Also,

since the $f_r(t)$ signal itself is a pulse train, it can be used directly for phase detection to achieve high precision. However, in order to obtain the speed error signal, an analogue speed signal (ω_r) is required for feedback application. Hence a frequency to voltage converter is adopted to convert f_r into the ω_r signal. In case, the corresponding conversion gain is unity, then the transfer function of G_{BLDC} is identical to G_P.

Next, consider the G_C block which consists of three inputs, namely ω_{er} and ω_s analogue signals as well as the f_r signal. However, there is only one analogue output, namely the desired equivalent armature current command i_s. From G_C block of Fig. 4.1 one can observe that the proposed controller basically combines a conventional PI control with a PLL control by using the *k* factor as coordination. The conventional PI control with k_P and 1-*k* parameters provides fast transient response but with limited speed control accuracy due to limited accuracy of analogue signals. Hence, an additional PLL control is added to enhance greatly the accuracy. In this block, the author adopts a tri-state phase frequency detector, namely PFD, to detect the phase difference between the command signal and the feedback signal. The feedback signal f_r is synthesized from the Hall-sensor signal. However, the command signal ω_s is an analogue signal. Hence, a voltage controlled oscillator, VCO, is used to convert ω_s signal into a comparable signal f_s for the tri-state PFD. The operation principle of the tri-state PF can be easily understood from the state transition diagram as shown in Fig. 4.3.

From Fig. 4.3 one can see that there are only three states, namely -1, 0, and +1 for the phase frequency detector. When each time the rising edge of command signal $f_s(t)$ is detected the present state is either moved to the next state to the right or remained in state +1. Similarly, each time the rising edge of feedback signal $f_r(t)$ is detected the present

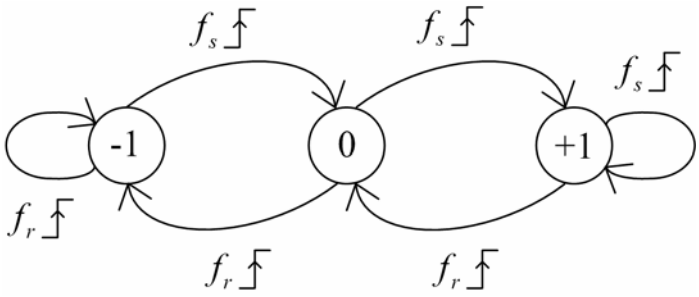

Fig. 4.3 State transition diagram of the PFD.

state is either moved to the next state to the left or remained in state -1. These three states are physically represented by three voltage levels. It is seen that through this detector one easily obtain very high accuracy speed error information. Also, to combine with the previous PI control component, a low pass filter is used to obtain an analogue value of the corresponding phase difference. As far as the physical meaning of the adopted PLL control is concerned, in spite of the pulse train signal form of f_s and f_r, since phase difference is the integral of its corresponding frequency error, the PLL controller is equivalent to an integral control. It is now quite clear that the proposed PLL assisted control is essentially a PI control where the integral control is decomposed into two parts. One is implemented in the analogue part with weighting factor 1-*k* and the other part is implemented in the PLL control with weighting factor *k*.

When the drive system is under transient or with large speed error (ω_{er}), then the proportional control will be dominant to achieve fast response, where the speed error is very small, the analogue I control can not provide good speed control accuracy, then the PLL control will be dominant to achieve high speed control accuracy. In other words, the resulting torque ripples and mechanical vibration noise will be greatly reduced. Also, when the command speed is adjusted, the coordinating factor *k*, if properly designed, will provide proper coordination between the PI control and the PLL control to achieve stable

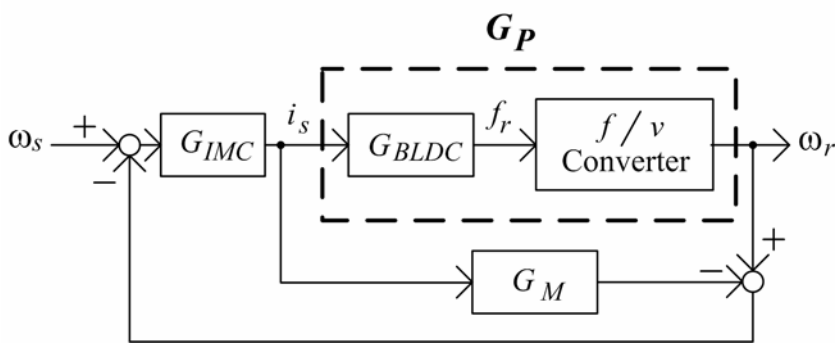

Fig. 4.4 The typical internal reference model control structure for the PMBLDC motor.

tracking of the speed command.

4.3 Derivation of Closed Form Expressions of k_P and k_I Parameters of the PI Controller

In order to obtain closed expressions of parameters k_P and k_I for convenient design of the PI controller, a robust internal model control [48-49] is adopted as a starting point of the derivation process. For completeness an internal reference model structure is shown in Fig. 4.4 [50] where a predictive internal model G_M is paralleled with the controlled plant G_P, which is the same as that in Fig. 4.1, and cascaded with an internal model controller G_{IMC}. To simplify Fig. 4.4 into a typical classical feedback control structure as shown in Fig. 4.5 where

$$G_C(s) = \frac{G_{IMC}(s)}{1 - G_{IMC}(s) \cdot G_M(s)} \tag{4.1}$$

The dynamic response, $\omega_r(s)$, of the whole system for speed command $\omega_s(s)$ then becomes:

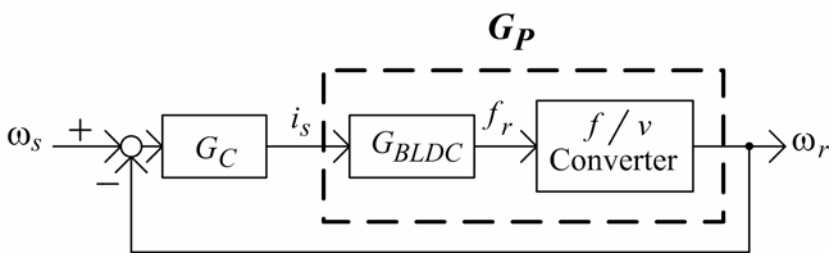

Fig. 4.5 The classic control structure for the PMBLDC motor.

$$\omega_r(s) = \frac{G_{IMC}(s) \cdot G_p(s)}{1 + [G_p(s) - G_M(s)] \cdot G_{IMC}(s)} \cdot \omega_s(s) \tag{4.2}$$

If $G_M(s) = G_P(s)$, then there is no feedback. Hence, the close-loop system will be stable if and only if $G_P(s)$ and $G_{IMC}(s)$ are stable. Under this case, $G_{IMC}(s) = G_M^{-1}(s)$. In case $G_M(s)$ contains time delay or right-half plane zeros, then for the sake of stability, one can factor $G_M(s)$ [50] as follows:

$$G_M(s) = G_{M^+}(s) \cdot G_{M^-}(s) \tag{4.3}$$

where $G_{M^+}(s)$ includes all zeros in the right-half plane and all time delays, and $G_{M^-}(s)$ is the remaining part such that its inverse is stable. Then, one can choose [50]

$$G_{IMC}(s) = G_{M^-}^{-1}(s) \cdot F(s) \tag{4.4}$$

where $F(s)$ is a low-pass filter. Thus, considering the PMBLDC motor system with the time delay, τ_L, one can obtain a time delayed model of $G_P(s)$ from (2.23) as follows:

$$G_P(s) = \frac{2\lambda_m}{Js + B} e^{-\tau_L s} \triangleq \frac{k_s e^{-\tau_L s}}{1 + T_p s} \tag{4.5}$$

where $T_p = J / B$, $k_s = 2\lambda_m / B$. One can choose a first order filter as

$$F(s) = \frac{1}{1 + T_f s} \tag{4.6}$$

It follows from (4.4) to (4.6) that the desired $G_{IMC}(s)$ becomes

$$G_{IMC}(s) = G_{M^-}^{-1}(s) F(s) = \frac{1 + T_p s}{k_s} \cdot \frac{1}{1 + T_f s} \tag{4.7}$$

Also, from (4.1) one can get

$$G_C(s) = \frac{1 + T_p s}{k_s (1 + T_f s) - k_s e^{-\tau_L s}} \tag{4.8}$$

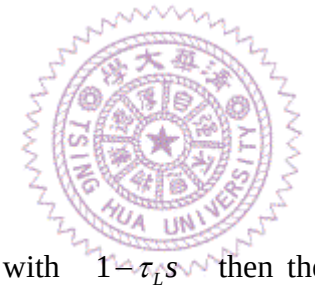

In case $e^{-\tau_L s}$ is approximated with $1 - \tau_L s$ then the resulting approximated $G_C(s)$, namely $G_{CA}(s)$ will become a classic PI controller as follows:

$$G_{CA}(s) = \frac{T_p}{k_s (\tau_L + T_f)} (1 + \frac{1}{T_p s}) \triangleq k_P + \frac{k_I}{s} \tag{4.9}$$

Then the corresponding closed expression form of k_P and k_I parameters will thus be:

$$k_P = T_p / [k_s (\tau_L + T_f)] \tag{4.10}$$

$$k_I = 1 / [k_s (\tau_L + T_f)] \tag{4.11}$$

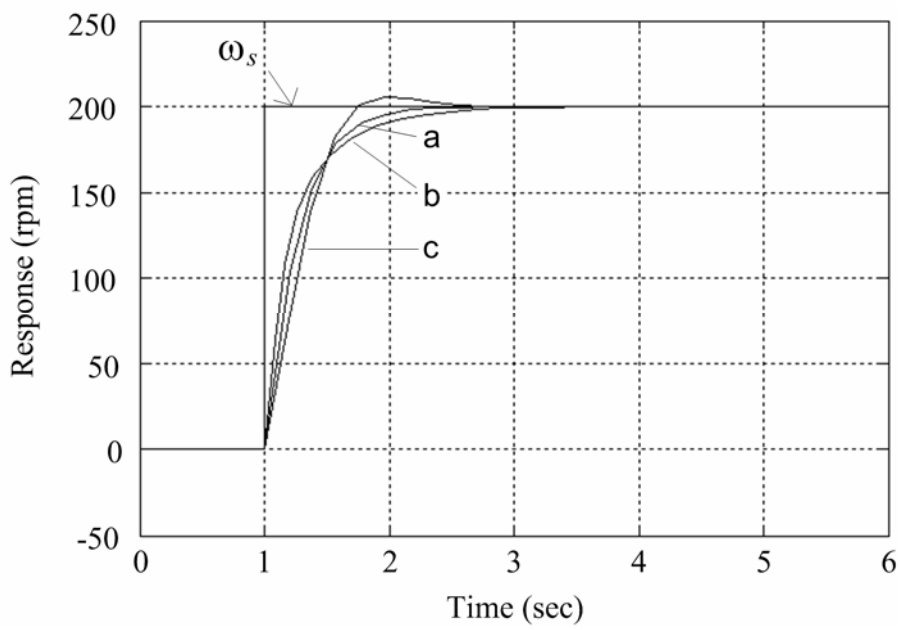

Fig. 4.6 Speed response simulations of the proposed system for different time constant T_p. (a) T_p=0.2sec. (b) T_p=0.3sec. (c) T_p=0.1sec.

For validate the robustness of the internal reference model, the transient simulations with different value of system parameter T_p are made. Consider the transient simulations of the drive system which is started from rest at $t=1$ sec. with a unit step speed command of 200rpm. Three cases, corresponding to the system parameters of $T_p = 0.2\,\text{sec.}$, $1.5T_p$ and $0.5T_p$ respectively are tested and the simulation results are shown in Fig.4.6. From Fig. 4.6 one can see the robust characteristic of the proposed control for ±50% variations of system parameter.

4.4 Stability Analysis of the Closed-Loop System

It is seen from Fig. 4.1 that when the drive system is controlled within the lock-in range, the $(1-k)/s$ branch can be merged with the PLL loop such that the total system

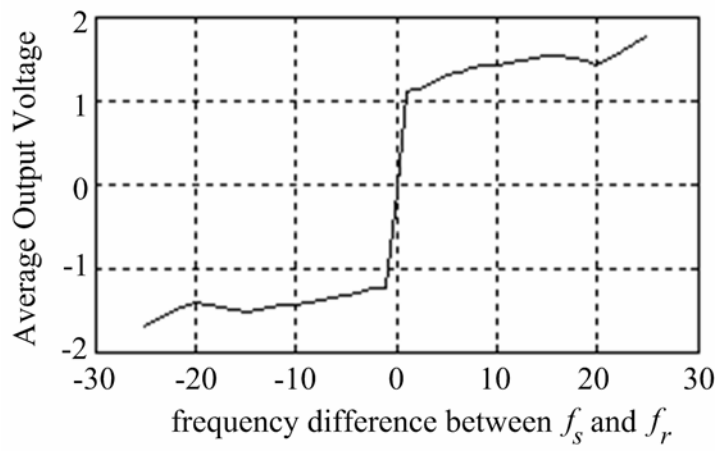

(a)

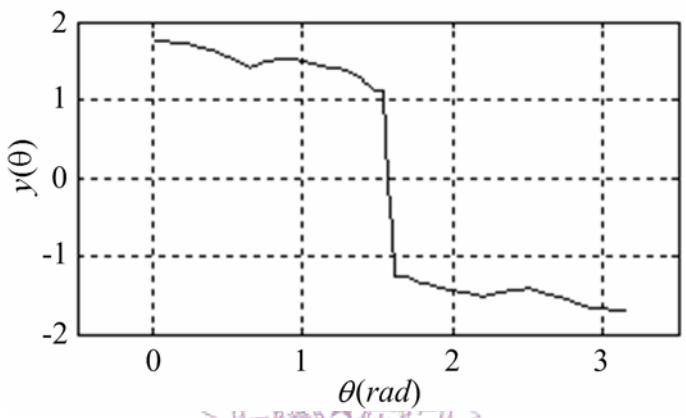

(b)

Fig. 4.7 (a) Average output voltage of 4046 PFD with the input of frequency difference between f_s and f_r under unlocked condition. (b) Output curve of PFD with the $cos\theta$ input under unlocked condition.

will function as an accurate PI controller. On the other hand, when under unlocked condition, the nonlinear characteristic of the PFD can be described using a describing function $D(x)$ whose average output voltage versus frequency difference between f_s and f_r is plotted in Fig. 4.7(a). In order to obtain an equivalent model of this nonlinear characteristic of the PFD under unlocked condition, one can use the same technique as [51]

by applying a sinusoidal signal $x(\theta) = cos\theta$ to serve as an equivalent input of the PFD. Thus, according to the input-output characteristic of PFD under unlocked condition as shown in Fig. 4.7(a), the corresponding output, say $y(\theta)$ of the PFD can be obtained as shown in Fig. 4.7(b). It follows that, as far as the fundamental frequency component is concerned, the resulting model of the PFD (IC4046) can be described by the simple input-output relationship, namely $y(\theta) \cong k_d x(\theta) = 1.987 x(\theta)$. Therefore, under transient condition, the PFD controller would act as a proportional controller as $D(\omega_{er}) = k_d$ in Fig. 4.8. However, it is interesting to see that under unlocked condition, application of the angular frequency difference to the PFD will result in an equivalent average phase difference (or phase error θ_e). Therefore, the resulting describing function model $D(\omega_{er})$ in Fig. 4.8 could be thought as an integrator physically.

From Fig. 4.8 one can calculate the steady state error $\omega_{er}(s)$ due to step input ω_s / s as follows:

$$\begin{aligned}\omega_{er}(s) &= \frac{\omega_s}{s} \times \frac{1}{1+G(s)} = \frac{\omega_s(\tau_L + T_f)(1+T_p s)}{s\{(\tau_L + T_f)(1+T_p s) + [T_p + kD(\omega_{er}) + \frac{(1-k)}{s}](1-\tau_L s)\}} \\ &= \frac{\omega_s(\tau_L + T_f)(1+T_p s)}{\Delta(s)}\end{aligned} \tag{4.12}$$

where ω_s is the command, $G(s)$ is the transfer function of the dotted square part in Fig. 4.8 and the denominator of the error function, namely , $\Delta(s)$ is defined as:

$$\Delta(s) = a_2 s^2 + a_1 s + a_0 \tag{4.13}$$

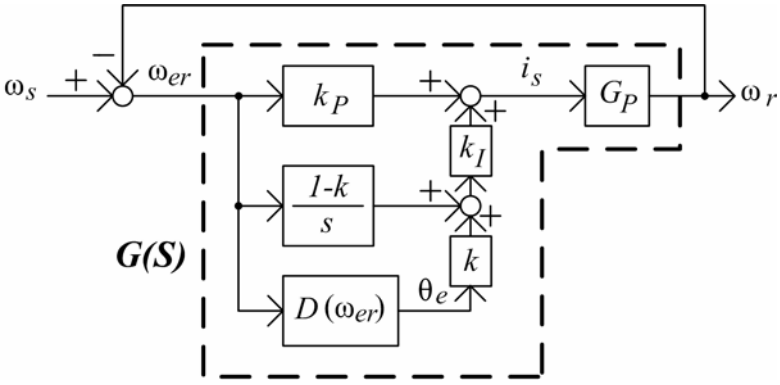

Fig. 4.8 The proposed PLL assisted speed controller of the PMBLDC with describing function D(ω_{er}).

where the coefficients of $\Delta(s)$ are given as follows:

$$a_2 = T_p T_f - \tau_L k D(\omega_{er}) \tag{4.14}$$

$$a_1 = T_p + T_f + k\tau_L + kD(\omega_{er}) > 0 \tag{4.15}$$

$$a_0 = 1 - k > 0 \tag{4.16}$$

In order to achieve zero steady state error, all poles of $\omega_{er}(s)$ in (4.12) should be located on the left-half complex plane. According to the Routh-Hurwitz criterion and given $a_2 > 0$, $a_1 > 0$ and $a_0 > 0$ one has the following criterion to achieve a stable condition.

$$T_f > \frac{k k_d \tau_L}{T_p} \tag{4.17}$$

Furthermore, from the loop gain $G(s)H(s)$ of Fig. 4.7 with $H(s) = 1$, one can get

$$G(s)H(s) = [k_P + kk_I D(\omega_{er}) + \frac{(1-k)k_I}{s}]G_p(s)$$
$$= [k_P + kk_I k_d + \frac{(1-k)k_I}{s}]\frac{k_s(1-\tau_L s)}{1+T_p s} \quad (4.18)$$

It follows that

$$G(j\omega)\cdot H(j\omega) = [k_p + kk_I k_d + \frac{(1-k)k_I}{j\omega}]\frac{k_s(1- j\omega\tau_L)}{1+ j\omega T_p}$$
$$= \frac{k_s[k_p + kk_I k_d]}{1+\omega^2 T_p^2}[(1-\omega^2\tau_L T_p) - j\omega(T_p + \tau_L)] \quad (4.19)$$
$$+ \frac{k_s k_I(1-k)}{\omega(1+\omega^2 T_p^2)}[-\omega(T_p + \tau_L) - j(1-\omega^2\tau_L T_p)]$$

$$\mathrm{Re}\{G(j\omega)\cdot H(j\omega)\} = \frac{k_s k_I}{1+\omega^2 T_p^2}[-\omega^2\tau_L T_p(T_p + kk_d) + kk_d - \tau_L + kT_p + K\tau_L] \quad (4.20)$$

$$\mathrm{Im}\,g\{G(j\omega)\cdot H(j\omega)\} = -\frac{k_s k_I}{\omega(1+\omega^2 T_p^2)}[\omega^2(T_p^2 + kk_d\tau_L + kk_d T_p + k\tau_L T_p) + 1 - k] \quad (4.21)$$

where $\mathrm{Re}\{G(j\omega)\cdot H(j\omega)\}$ and $\mathrm{Im}\,g\{G(j\omega)\cdot H(j\omega)\}$ are the real and imaginary parts of the loop gain respectively. From (4.19), one can let $\mathrm{Im}\,g\{G(j\omega_p)\cdot H(j\omega_p)\}$ be equal to zero to get the desired gain margin, Gm, of the system

$$Gm = 1 + \mathrm{Re}\{G(j\omega_p)\cdot H(j\omega_p)\} = \frac{T_p T_f - kk_d\tau_L}{T_p(T_f + \tau_L)} \quad (4.22)$$

Next assume $\left|G(j\omega_g)\cdot H(j\omega_g)\right| = 1$, then the phase margin, Pm, of the system can be obtained

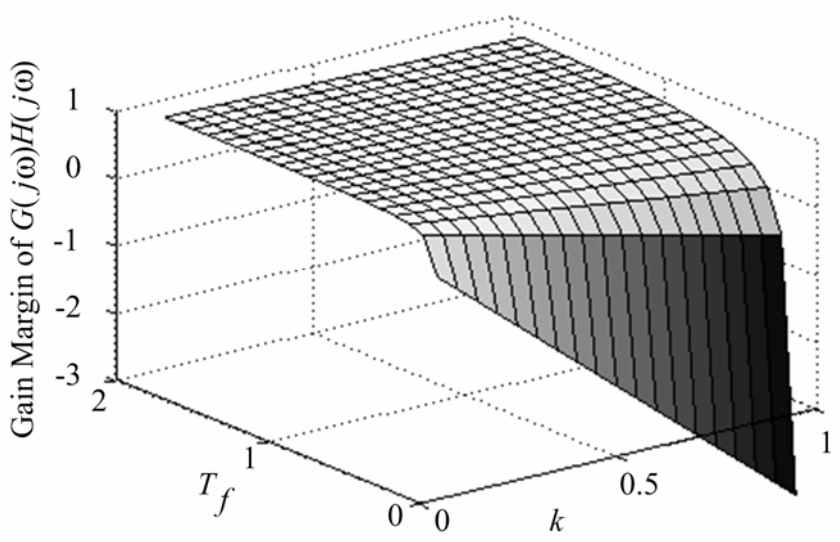

Fig. 4.9 Stability margin for the variation of system parameters k and T_f of the proposed controller.

$$Pm = \tan^{-1}\left(\frac{\mathrm{Im}\, g(G(j\omega_g)\cdot H(j\omega_g))}{\mathrm{Re}(G(j\omega_g)\cdot H(j\omega_g))}\right) + \pi \tag{4.23}$$

Therefore the relative stability, Gm and Pm, could be derived according to (4.22) and (4.23) at the phase-crossover frequency, ω_p, and gain-crossover frequency, ω_g, respectively. Again, the critical criterion which separates the stable system from the unstable one is

$$Gm = \frac{T_p T_f - k k_d \tau_L}{T_p (T_f + \tau_L)} > 0 \tag{4.24}$$

According to (4.24), one can obtain the consistent stability criterion as (4.17).

From the loop gain margin function shown in (4.22), one can examine the sensitivities of parameters k and T_f to the proposed control system on the relative stability. The

simulation result is shown in Fig. 4.9. From Fig. 4.9, one can observe that to achieve better stability T_f should be larger while *k* should be kept smaller.